

## Supporting Information

### Synergic effect of Ni-NiMo<sub>4</sub>N<sub>5</sub> nitride heterostructure and Fe-doping enables active and durable alkaline water splitting at the industrial current density

Yaling Zhao,<sup>a,b</sup> Jinsheng Li,<sup>a</sup> Kai Li,<sup>c</sup> Liang Liang,<sup>a</sup> Jianbing Zhu,<sup>a,b\*</sup> Meiling Xiao,<sup>a,b\*</sup> Changpeng Liu,<sup>a,b\*</sup>  
Wei Xing<sup>a,b\*</sup>

#### Experimental Section

**Chemicals.** Nickel foam (NF, thickness 0.3 mm, porosity 95%), Nickel nitrate hexahydrate (97%), Ammonium molybdate tetrahydrate (99%), and Ferric nitrate nonahydrate were gained from Innochem. Potassium hydroxide (KOH, 86%) and Ethanol (99.7%) were purchased from Xihua. Platinum carbon black (Pt/C, 40%), and Nafion solution (5%) were purchased from Sigma-Aldrich. The deionized water in the experiment is always ultrapure water (18.2 mΩ·cm).

**Synthesis of pre-NiFeMo.** First, the NF was cut into a rectangular shape with the size of 1\*6 cm<sup>2</sup>. Second, the pieces of NF were washed with 3 M HCl, ethanol, and deionized water, respectively. 1.2 mmol Nickel nitrate hexahydrate, 0.1 mmol Ammonium molybdate tetrahydrate, and 0.15 mmol Ferric nitrate nonahydrate were dissolved in 30 mL of deionized water and sonicated to yield a transparent solution. This solution was subsequently transferred into a 50 mL autoclave. The preprocessed NF was then placed inside the autoclave and reacted at a temperature of 150°C for 8 hours. After the hydrothermal reaction, the NF was rinsed with deionized water and dried again at 60°C in an oven for 10 hours to gain the pre-NiFeMo/NF.

**Synthesis of pre-NiMo.** The preparation method is identical to the pre-NiFeMo/NF, except without the addition of iron nitrate.

**Synthesis of NiMo-NH<sub>3</sub>, and NiFeMo-NH<sub>3</sub>.** The pre-NiMo and NiFeMo/NF were put into a tube furnace where they were annealed in ammonia at 500°C for 3 h at an increasing rate of 2.5°C min<sup>-1</sup>. After cooling down, the desired catalysts were obtained.

**Synthesis of NiFeMo-Ar, and NiFeMo-Air.** The pyrolysis process is identical to the NiMo-NH<sub>3</sub> and NiFeMo-NH<sub>3</sub>, with the exception that the pyrolysis atmospheres become Ar and Air, respectively.

## Structural Characterizations

X-ray diffraction (XRD) patterns were recorded on a Nikaku Smartlab 9kw Cu target,  $K\alpha$  radiation ( $\lambda=0.15406$  nm), operating voltage and current of 45 kV and 100 mA, respectively. The micromorphology and structure were characterized by scanning electron microscopy (SEM, Philips XL 30 ESEM-FEG), and high-resolution transmission electron microscopy (HRTEM, FEI Talos F200S) equipped with the energy dispersive X-ray spectrometer (EDS, QUANTAX). The surface species were analyzed by X-ray photoelectron spectroscopy (XPS, ThermoFisher Escalab 250Xi) with an Al X-ray source at 150 W. Inductively coupled plasma optical emission spectroscopy (ICP-OES; X Series 2, Thermo Scientific USA) was used to determine the ratio of metal atoms.

## Electrochemical measurements

The electrochemical performance of the as-prepared catalysts was measured in a standard three-electrode cell using CHI 760E (CH Instrument). Typically, a carbon rod and a Hg/HgO electrode containing 1M KOH internal aqueous solution were used as the counter electrode and reference electrode respectively.  $N_2$  saturated 1 M KOH was used as the electrolyte. All potentials in this study are given referenced with a reversible hydrogen electrode (RHE) according to the following equation:

$$E(\text{vs. RHE}) = E(\text{vs. Hg/HgO}) + 0.923 \text{ V}$$

where 0.923 V is the potential difference between the Hg/HgO reference electrode and RHE in 1 M KOH, which was calibrated by the CV test prior to electrocatalysis.

The linear sweep voltammetric (LSV) curves were tested at the scan rate of 1 mV/s (iR-corrected). The Tafel slope is obtained by linearly fitting the points in the Tafel region of the LSV data. Electrochemical impedance spectra Nyquist plots were measured at an overpotential of 0 V from 10 kHz to 0.1 Hz.

## In situ Raman measurements

The in situ Raman spectra were obtained on a high-speed and high-resolution confocal Raman spectrometer (HORIBA LabRAM Odyssey™). The experiments were performed in a tailor-made Raman spectro-electrochemical cell. A 50x microscope objective was used. The excitation wavelength of the laser was 532 nm. A silica wafer was used to calibrate the Raman frequencies. The potential was controlled by a Bio-Logic EC-LAB potentiostat.

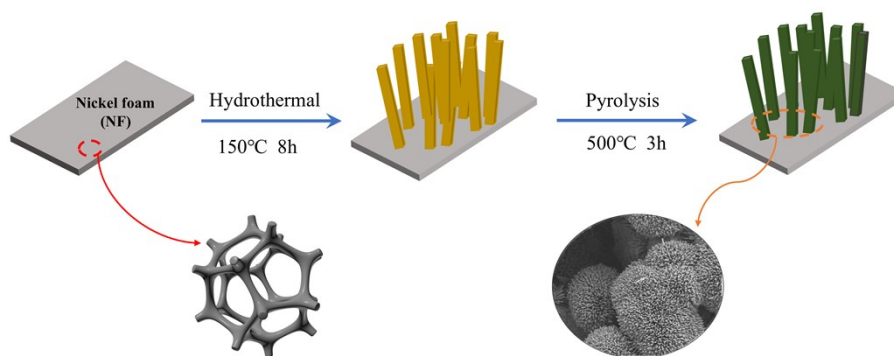


Figure S1. Schematic illustration of the synthesis procedures.

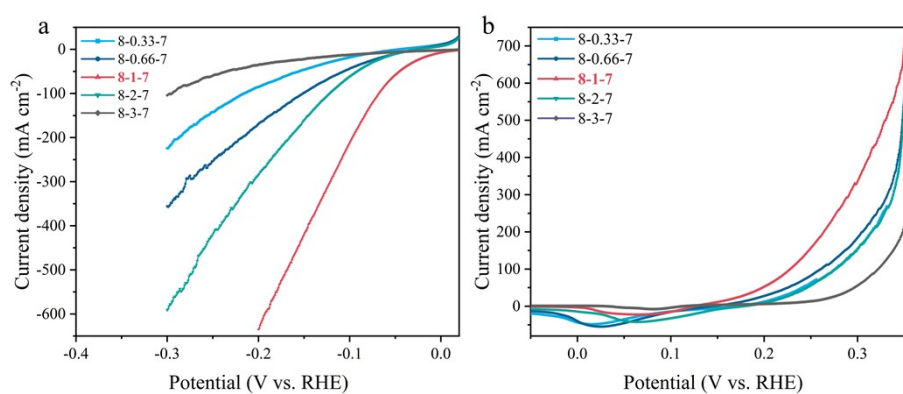


Figure S2. (a) HER and (b) OER polarization curves of NH<sub>3</sub>-treated samples with different Fe contents in 1 M KOH electrolytes.

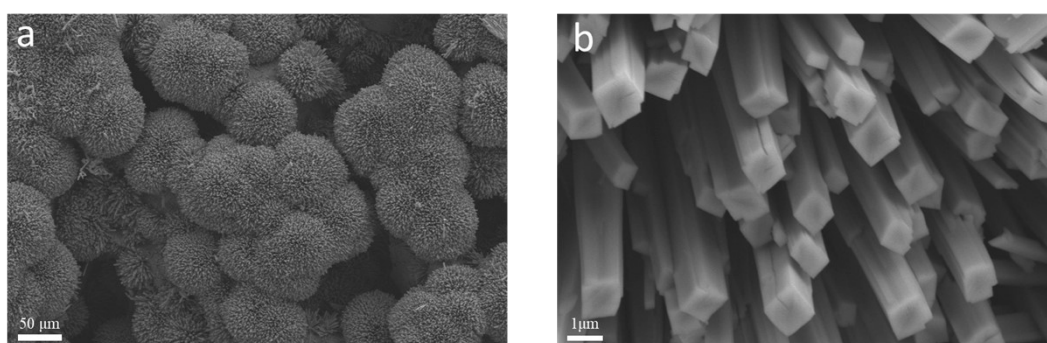


Figure S3. SEM images of NiMo-NH<sub>3</sub>.

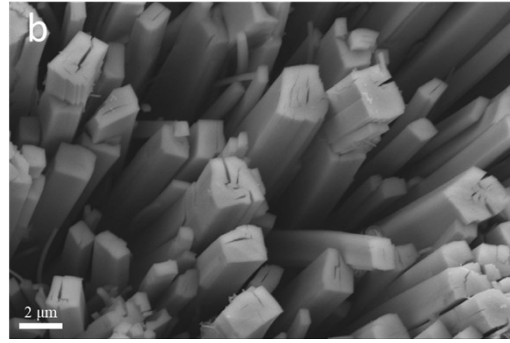


Figure S4. SEM images of NiFeMo-NH<sub>3</sub>.

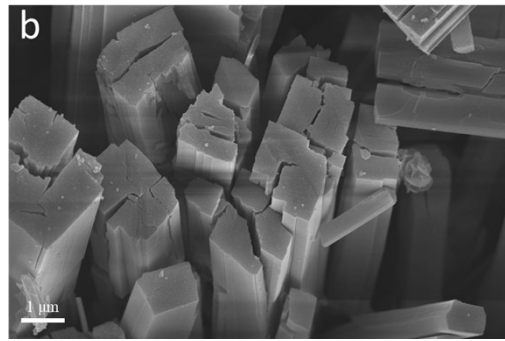
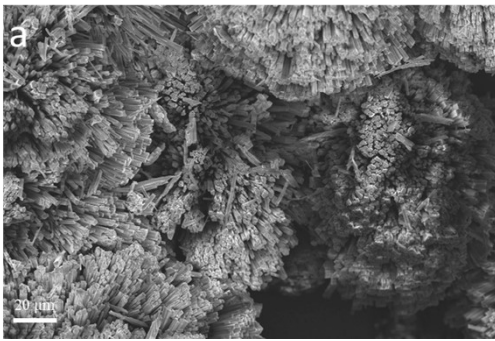


Figure S5. SEM images of NiFeMo-Ar.

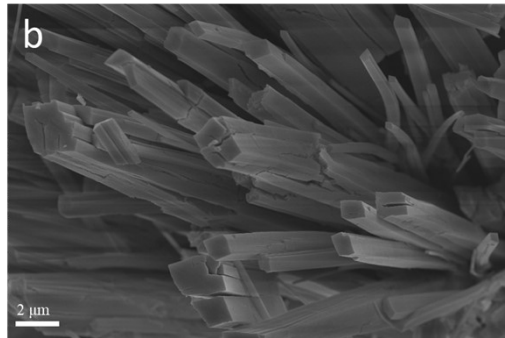
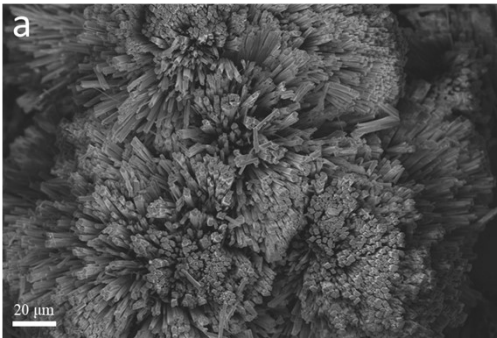


Figure S6. SEM images of NiFeMo-Air.

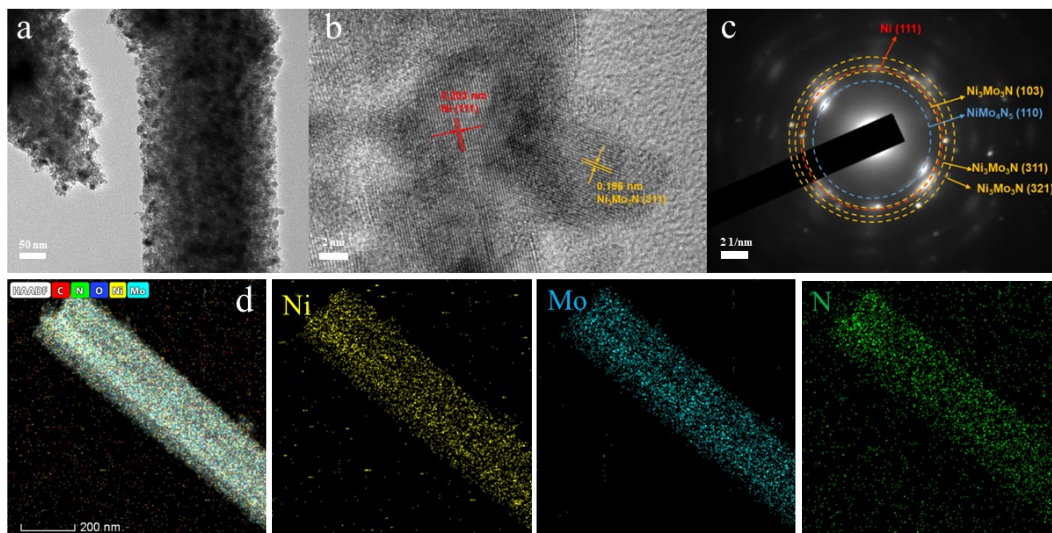


Figure S7. Morphology and structure characterizations. (a, b) High-resolution transmission electron microscopy (HRTEM), (c) selected area electron diffraction image (SAED), and (d) the corresponding EDS images of NiMo-NH<sub>3</sub>.

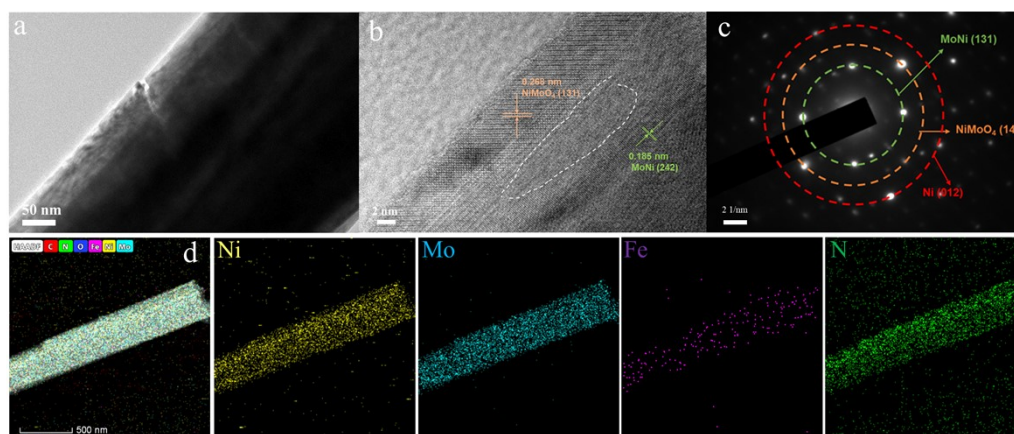


Figure S8. Morphology and structure characterizations. (a, b) High-resolution transmission electron microscopy (HRTEM), (c) selected area electron diffraction image (SAED), and (d) the corresponding EDS images of NiFeMo-Ar.

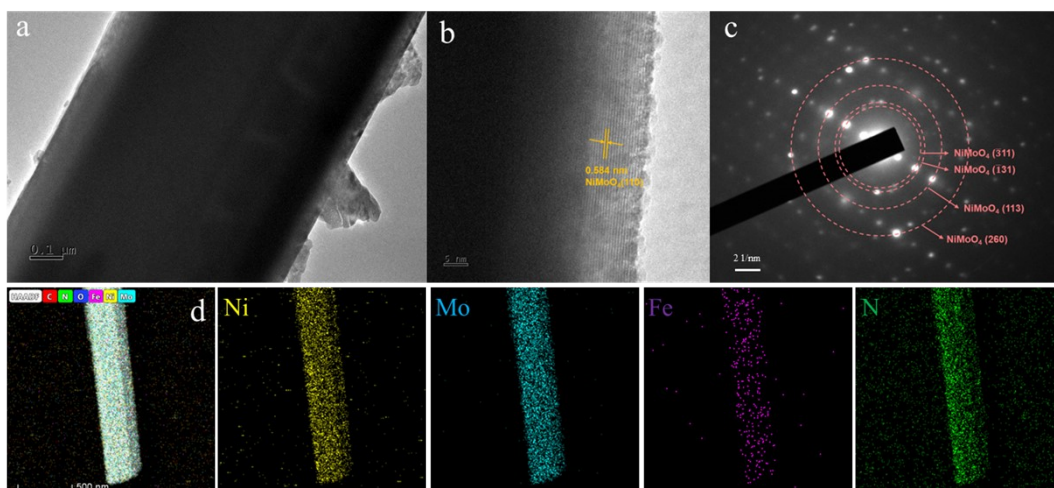


Figure S9. Morphology and structure characterizations. (a, b) High-resolution transmission electron microscopy (HRTEM), (c) selected area electron diffraction image (SAED), and (d) the corresponding EDS images of NiFeMo-Air.

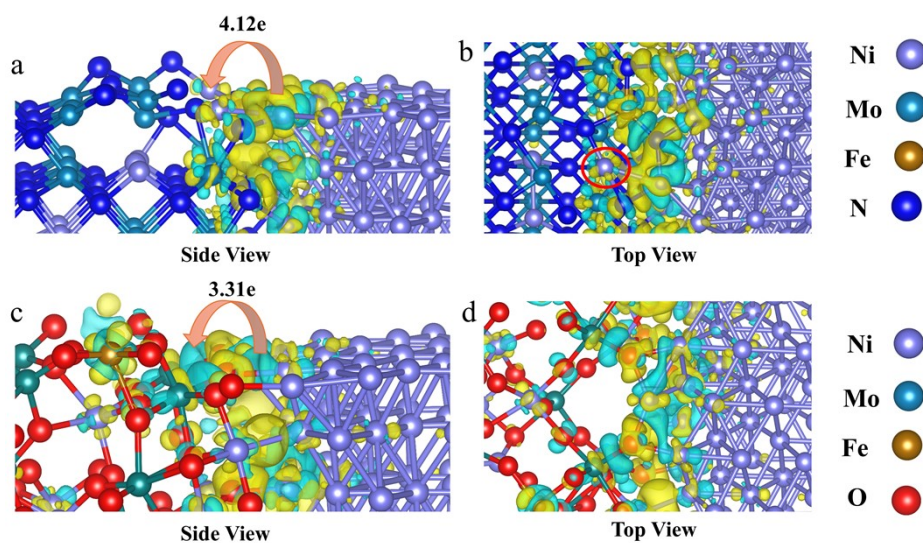


Figure S10. Bader charge density analysis, (a) the side view and (b) the top view of Fe-doping Ni-NiMo<sub>4</sub>N<sub>5</sub> interface, (c) the side view and (d) top view of Fe-doping Ni-NiMoO<sub>4</sub> interface, yellow represents the gain of electrons, while blue represents the loss of electrons.

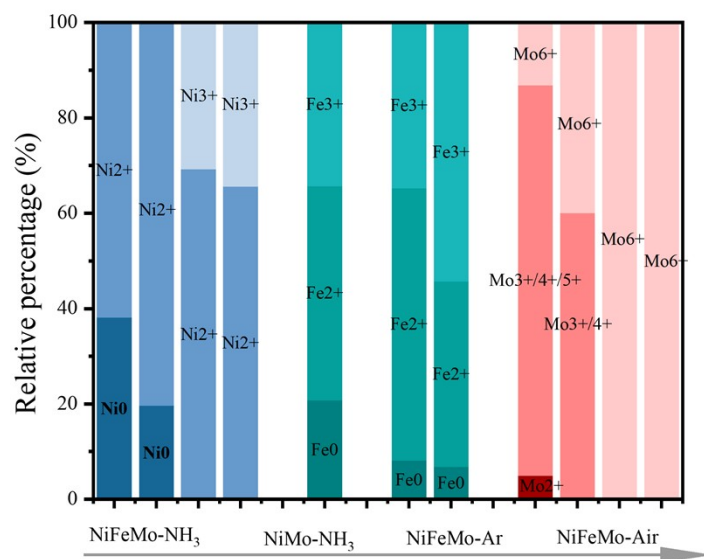


Figure S11. The proportion of metal valences of four prepared catalysts.

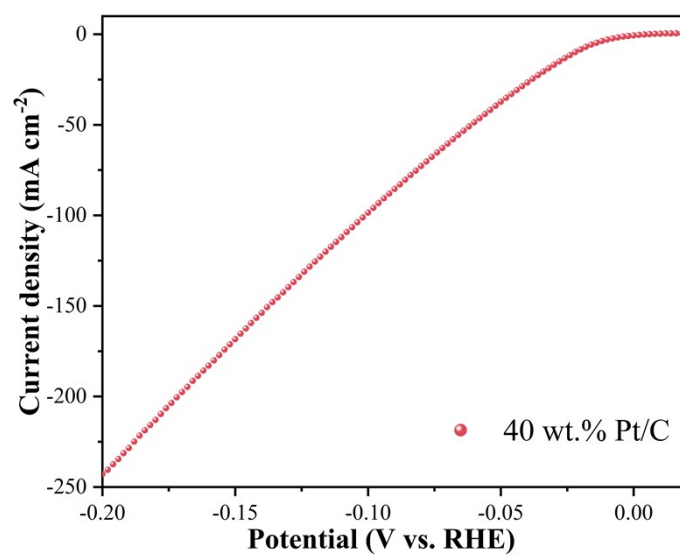


Figure S12 The HER polarization curve of Pt/C.

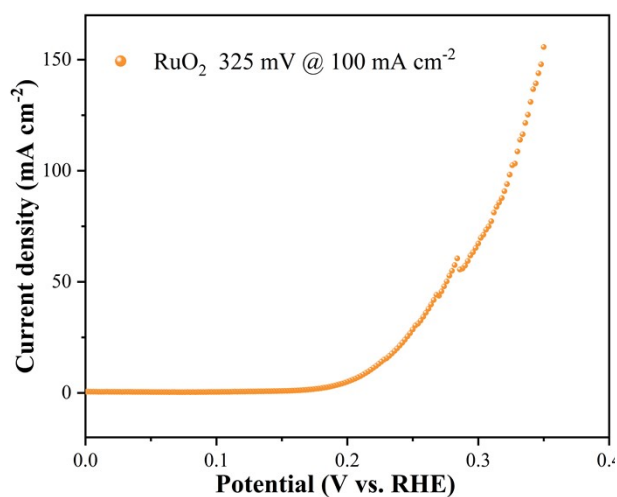


Figure S13 The OER polarization curve of RuO<sub>2</sub>.

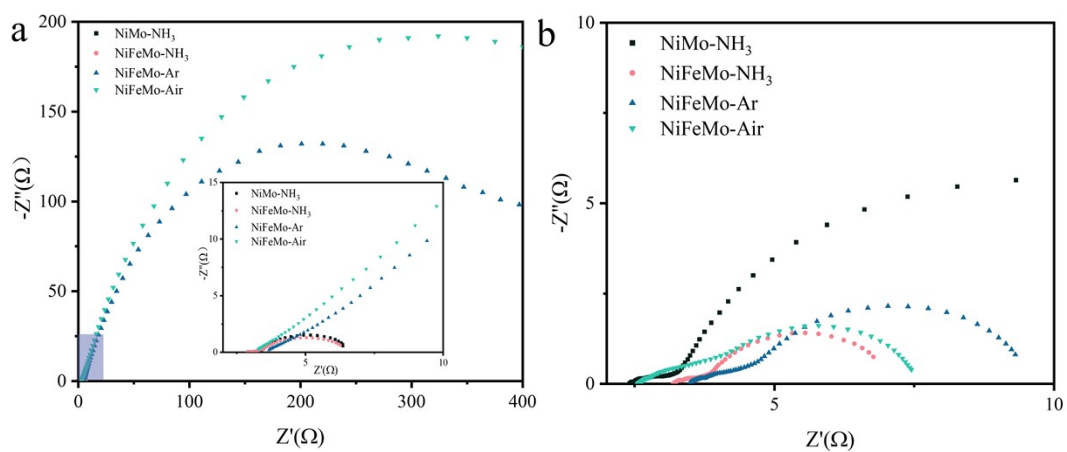


Figure S14. Nyquist diagrams for a) HER and b) OER process.

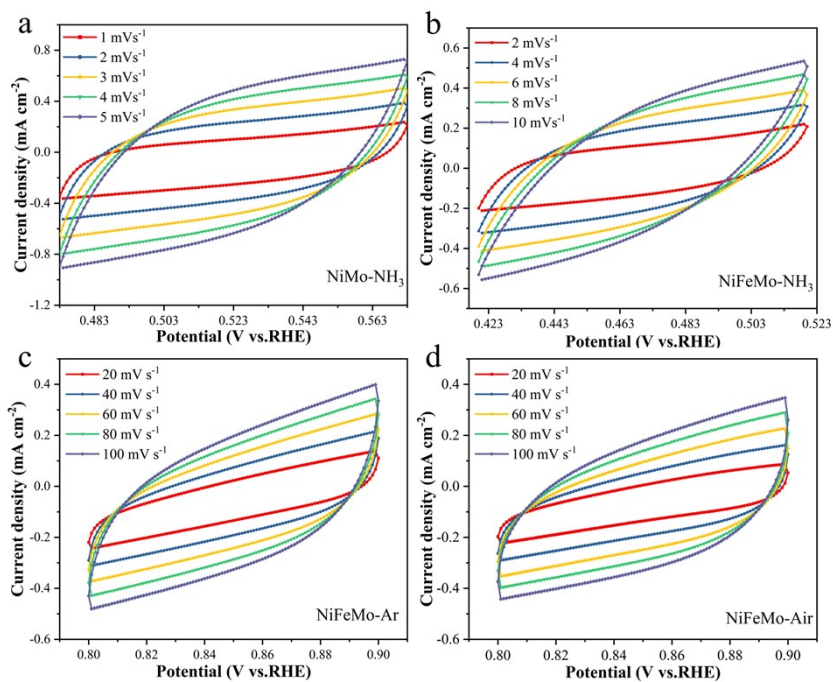


Figure S15. CV curves under different scan rates for estimation of  $C_{dl}$ .

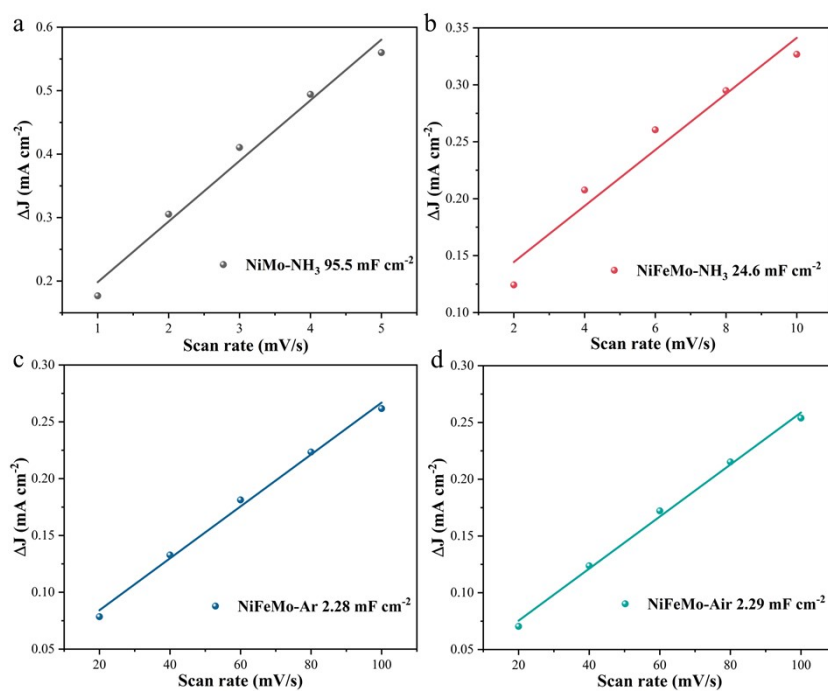


Figure S16. Calculation of double-layer capacitance ( $C_{dl}$ ).

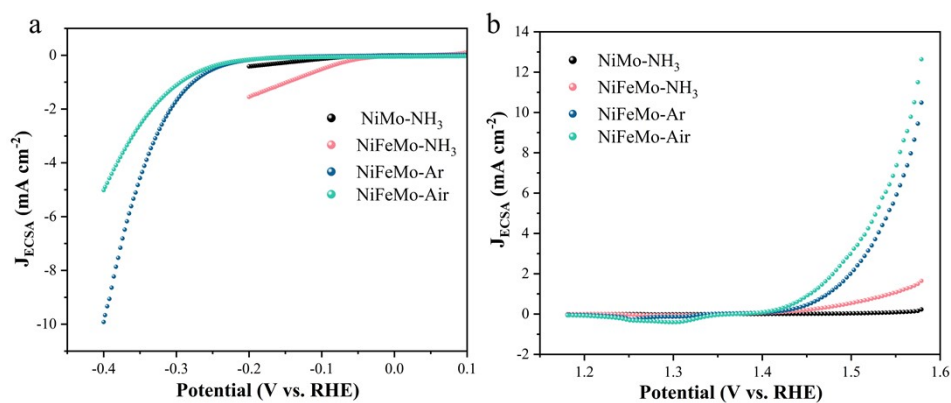


Figure S17 (a) HER and (b) OER ECSA normalized polarization curves.

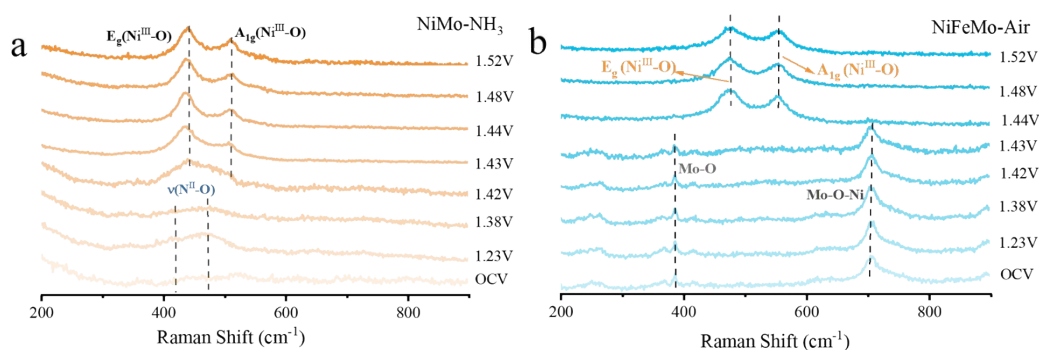


Figure S18. In situ Raman spectra measurements at different potentials (from OCV to 1.52 V vs. RHE) in 1 mol/L KOH electrolyte with (a) NiMo-NH<sub>3</sub> and (b) NiFeMo-Air as the anode.

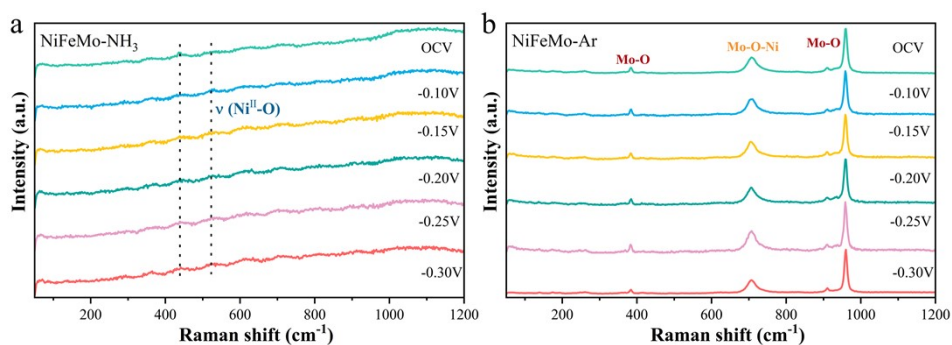


Figure S19 In-situ Raman spectroscopy tests for structural transformations of (a) NiFeMo-NH<sub>3</sub> and (b) NiFeMo-Ar during alkaline HER process.

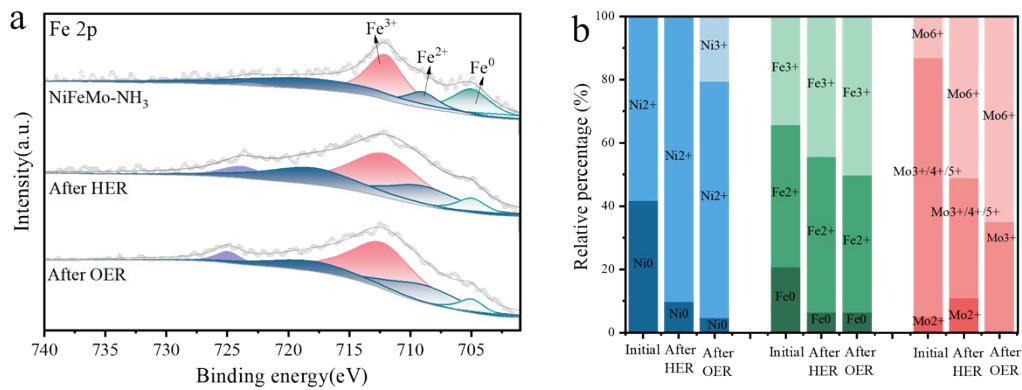


Figure S20. XPS of (a) Fe 2p and (b) the proportion of metal valences after 10000 cycles ADT tests for HER and OER in comparison with initial states of NiFeMo-NH<sub>3</sub>.

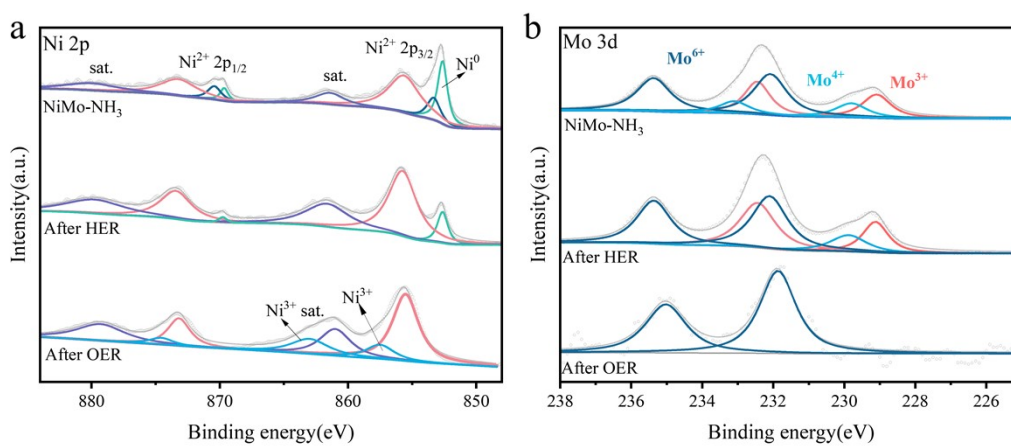


Figure S21 XPS of (a) Ni 2p, and (b) Mo 3d of NiMo-NH<sub>3</sub> after the HER and OER tests in comparison with before tests.

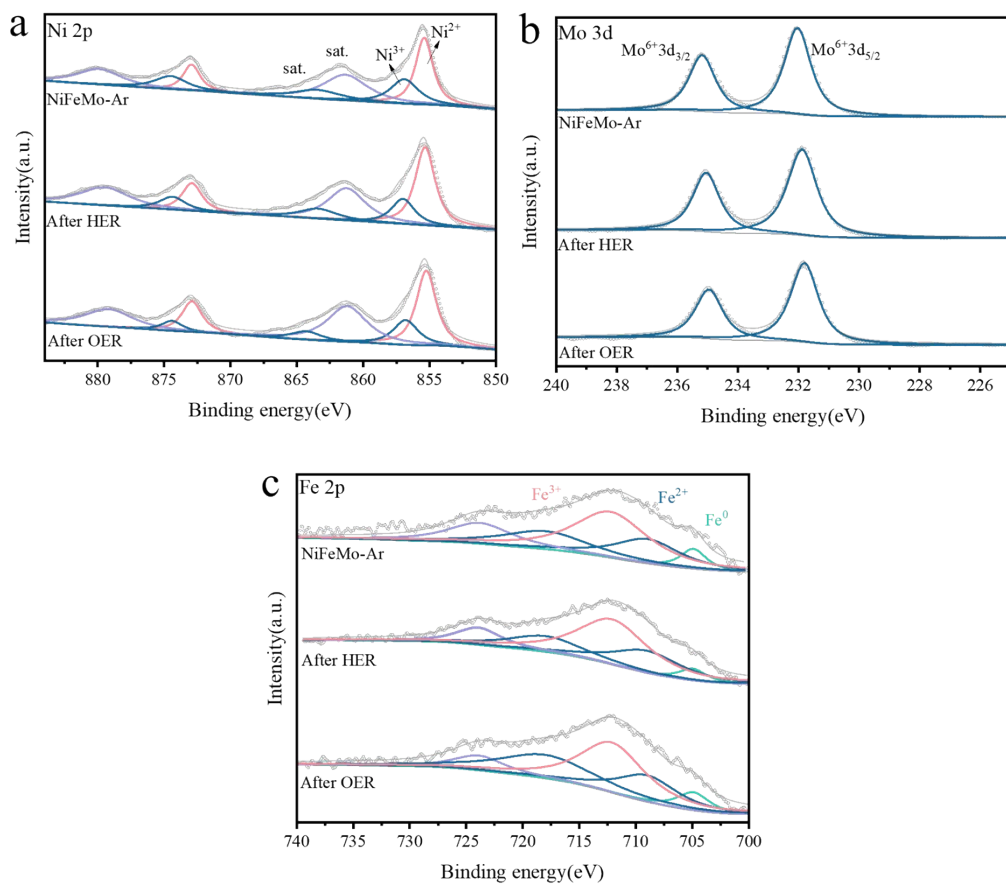


Figure S22. XPS of (a) Ni 2p, (b) Mo 3d, and (c) Fe 2p of NiFeMo-Ar after the HER and OER tests in comparison with before tests.

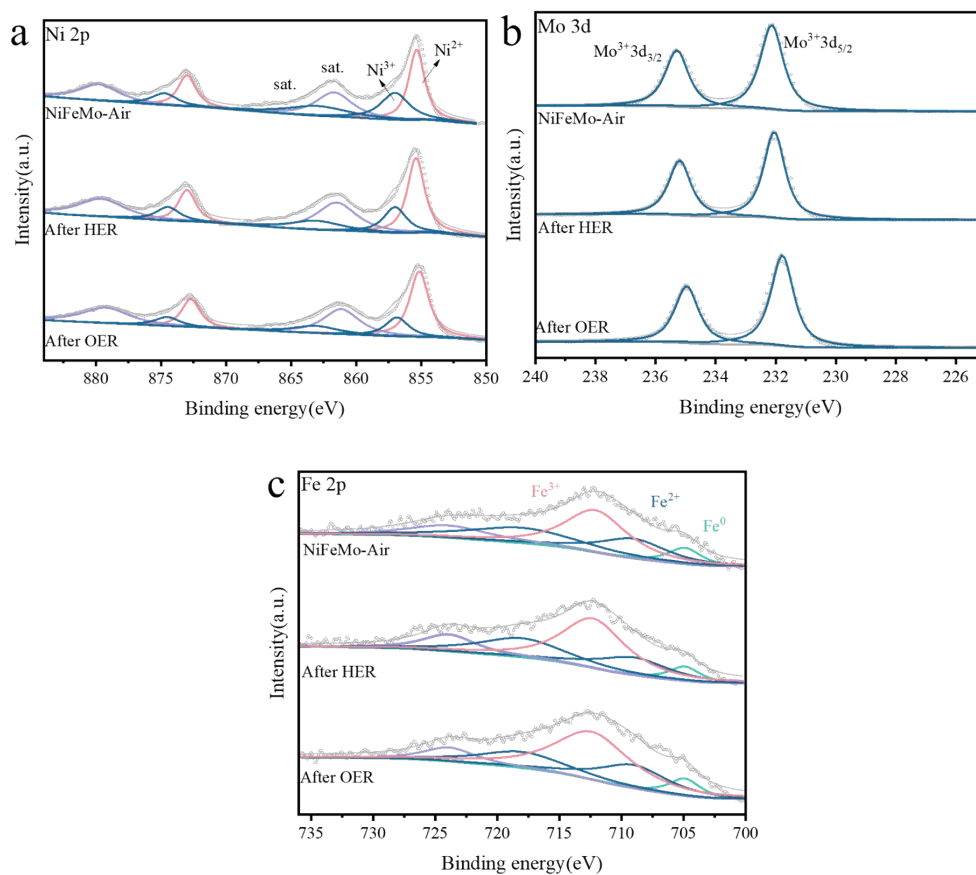


Figure S23. XPS of (a) Ni 2p, (b) Mo 3d, and (c) Fe 2p of NiFeMo-Air after the HER and OER tests in comparison with before tests.

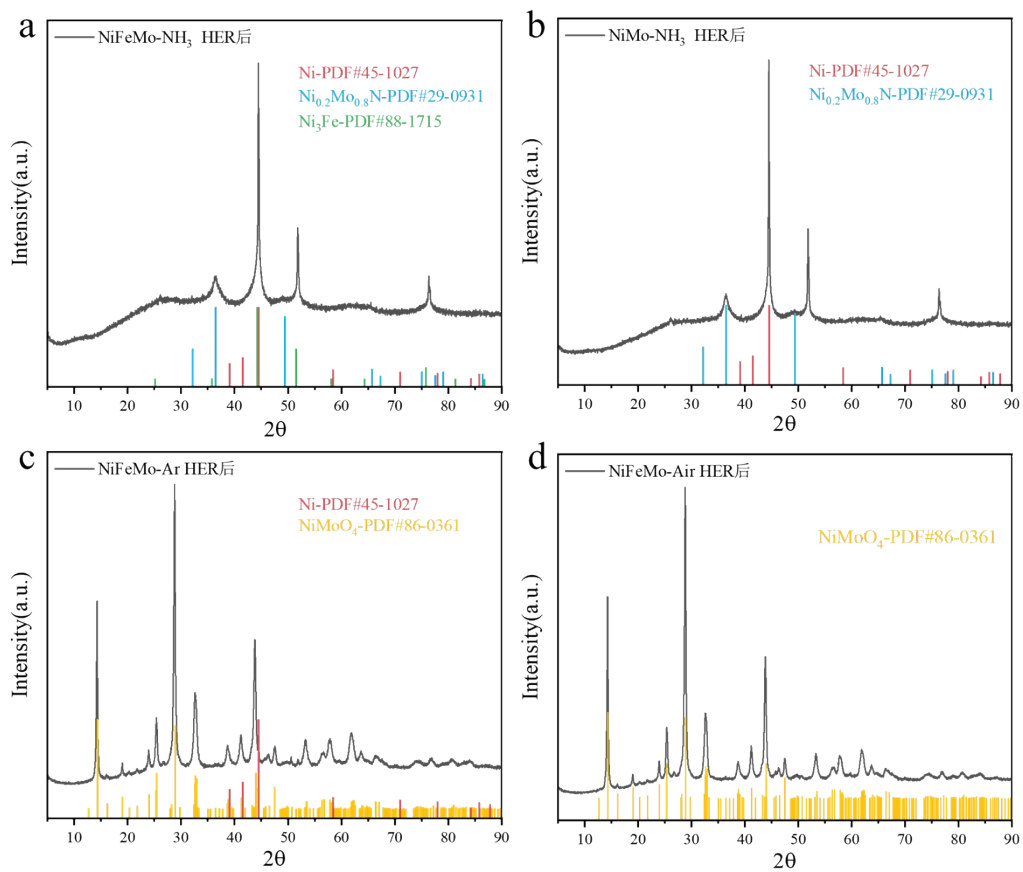


Figure S24. XRD pattern of the catalysts along with the standard PDF cards after HER tests.

Table S1. The loadings of Ni, Fe, and Mo by ICP measurement

<b>Catalysts</b>	<b>Ni (wt%)</b>	<b>Fe (wt%)</b>	<b>Mo (wt%)</b>
NiFeMo-NH <sub>3</sub>	34	1.29	44.9
NiMo-NH <sub>3</sub>	34.52		45.04
NiFeMo-Ar	22.81	1.12	37.02
NiFeMo-Air	24.63	1.44	24.63